A LEVEL SET METHOD FOR ANISOTROPIC GEOMETRIC DIFFUSION IN 3D IMAGE PROCESSING

TOBIAS PREUSSER AND MARTIN RUMPF*

Abstract. A new morphological multiscale method in 3D image processing is presented which combines the image processing methodology based on nonlinear diffusion equations and the theory of geometric evolution problems. Its aim is to smooth level sets of a 3D image while simultaneously preserving geometric features such as edges and corners on the level sets. This is obtained by an anisotropic curvature evolution, where time serves as the multiscale parameter. Thereby the diffusion tensor depends on a regularized shape operator of the evolving level sets. As one suitable regularization local L^2 projection onto quadratic polynomials is considered. The method is compared to a related parametric surface approach and a geometric interpretation of the evolution and its invariance properties are given. A spatial finite element discretization on hexahedral meshes and a semi-implicit, regularized backward Euler discretization in time are the building blocks of the easy to code algorithm. Different applications underline the efficiency and flexibility of the presented image processing tool.

Key words. Image Processing, Level Set Method, Geometric Modeling, Curvature Evolution

AMS subject classifications. 53K55, 65U10, 65N30

1. Introduction. Multiscale methods have proved to be successful tools in image denoising, edge enhancement and shape recovery [1, 34, 39, 27]. Thereby, the image is considered as initial data of a suitable evolution problem. Time represents the scale parameter which leads from noisy fine scale to smoothed and enhanced coarse scale representations of the data. Processing three dimensional images is a task of growing interest in various applications. Especially in medical imaging different image generation hardware such as CT or MRI devices, and more recently also 3D ultrasound devices deliver large image data at high resolution for further post processing and analysis. These images and especially 3D ultrasound images are characterized by high frequent noise typically due to measurement errors. Often, one is interested in the extraction of certain level surfaces from the data, which bound volumes or separate regions of interest. Frequently the actual intensity value is of minor importance and dependent on the modality in the image generation process. Methods which behave invariant under transformations of the intensity or gray scale are called morphological. They only effect the morphology of the image, which coincides with the geometry of the level sets.

The aim of this paper is to discuss a new anisotropic level set method for the denoising of large, digital 3D images (cf. Section 4 and [10] for a related method on parametric surfaces as they typically appear in computer graphics). The peculiarity of the method is, that it is able to preserve edges and corners on level sets while still allowing tangential smoothing along the edges. Furthermore it is characterized by a rich class of invariant shapes. Indeed ellipsoids given as level sets of a quadratic polynomial are unaffected by the corresponding evolution.

Figure 1.1 gives a first glance on the performance of the new method and compares it with other methods: The new anisotropic geometric diffusion approach is characterized by substantial tangential smoothing, especially compared to the original Perona Malik scheme, and conserves sharp edges and details in the example much better than the anisotropic Perona Malik diffusion.

The core of the method is an evolution driven by *anisotropic geometric diffusion* of level surfaces. The anisotropic diffusion tensor depending on a presmoothed shape operator — and therefore depending on presmoothed principal curvatures and principal directions of cur-

* Faculty 4, Institute for Mathematics, University of Duisburg, Lotharstrasse 65, 47048 Duisburg, ([preusser, rumpf]@math.uni-duisburg.de)

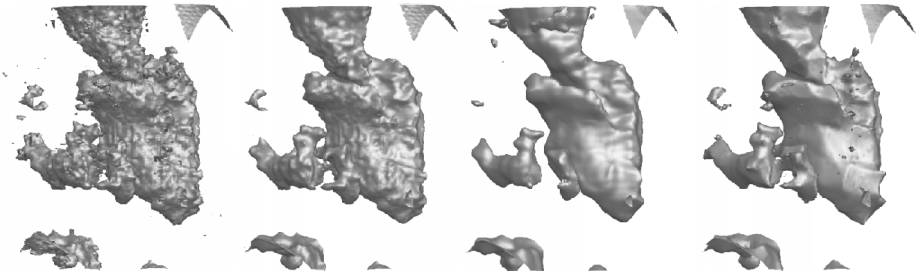

FIG. 1.1. A noisy 3D echocardiographical data set (left) is evolved by isotropic Perona Malik diffusion (middle left), anisotropic Perona Malik diffusion (middle right) and by the new anisotropic level set method (right). Snapshots depict one specific level set always at the same evolution time. The computation was performed on a 128^3 grid.

vature — is sensitive to the identification of the important surface features. It decreases the diffusivity in certain directions in close vicinity to edges or corners. Here we make us of the observation that edges on surfaces are indicated by one dominant and one sub-dominant principal curvature. The curvature direction corresponding to the dominant curvature can be considered as the tangential direction along the edge. Mainly two parameters are at the disposal of the user to influence the performance of the method:

- A threshold value λ related to principal curvatures which are assumed to indicate an edge and thus require local preservation and
- a filter width σ which controls the noise reduction on the actual surface before evaluating the shape operator.

The difference between the actual and the presmoothed shape operator plays an essential role in the control of the evolution problem. Furthermore, the built-in prefiltering is essential to make the proposed method robust and mathematically well-posed. In this paper we first present a continuous model, analyze and discuss its qualitative properties. Then in a second step we seek a robust and efficient discretization. Hence, we derive an appropriate finite element level set method with respect to a formulation of the continuous problem in variational form. Values on nodes of a hexahedral grid correspond to voxel values in the digital image. We find a finite element approach preferable compared to a finite difference discretization due to its intrinsic Galerkin structure, which simplifies the modeling and the study of the qualitative behavior. Recently, Deckelnick and Dziuk [11] proved convergence of the closely related finite element approximation for mean curvature motion in level set formulation to a viscosity solution of the continuous problem. Furthermore, in the finite element setting the anisotropy can be handled element-wise in a natural way. Based on concepts developed in [29] the computational cost even of an adaptive finite element scheme is comparable to a finite difference formulation with the same number of unknowns.

The paper is organized as follows. First, in Section 2 we discuss some background work on image processing, surface fairing and curvature flow. In the following Section 3 we briefly introduce some geometric notation. Then in Section 4 we review a parametric model for surface processing which has been presented recently [10]. It further motivates our modeling in the context of level sets. Section 5 gives a detailed description of the new method, whereas in Section 6 we discuss possible regularizations of the shape operator. Afterwards, in Sections 7 and 8 we present the actual discrete model. Finally, in Section 9 we compare the parametric and the level set model and draw conclusions in Section 10.

2. Review of related work. Let us consider a noisy image given by an intensity map $\phi_0 : \Omega \to \mathbb{R}$ on some image domain $\Omega \subset \mathbb{R}^3$. Scale space methods define an evolution oper-

ator $E(t)$ which acts on the image ϕ_0 and delivers a family of representations $\{E(t)\phi_0\}_{t\geq 0}$ on successively coarser scales. One of the first successful methods along this concept was presented by Perona and Malik [27]. They proposed a nonlinear diffusion method, which modifies the diffusion coefficient at edges, which are indicated by steep intensity gradients. For a given initial image ρ_0 they considered the evolution problem

$$\partial_t \rho - \mathrm{div}(G(\|\nabla\rho\|)\nabla\rho) = 0.$$

Here the time t acts as the scale parameter. For increasing t the original image at the initial time $t = 0$ is successfully smoothed and image patterns are coarsened. Simultaneously edges are enhanced if one chooses a diffusion coefficient $G(.)$ which suppresses diffusion in areas of high gradients. A suitable choice is $G(s) = \left(1 + s^2/\lambda^2\right)^{-1}$ for a positive constant λ. Thus, edges are classified by λ. I. e. sharpening by backward diffusion is invoked whenever $\|\nabla\rho\| \geq \lambda$ whereas the image is smoothed by forward diffusion for $\|\nabla\rho\| \leq \lambda$. Kawohl and Kutev [19] gave a detailed analysis of the diffusion types in this method. Unfortunately, the above original Perona and Malik model is still ill-posed because there is a true backward diffusion in areas of large gradients. Catté et al. [6] proposed a regularization method where the diffusion coefficient is no longer evaluated on the exact intensity gradient. Instead they suggested to consider the gradient evaluation on a prefiltered image, i.e., they consider the equation

$$\partial_t \rho - \mathrm{div}(G(\|\nabla\rho_\sigma\|)\nabla\rho) = 0 \tag{2.1}$$

where $\rho_\sigma = K_\sigma * \rho$ with a suitable local convolution kernel K_σ of width σ. For instance we may use a Gaussian filter kernel. This model turns out to be well-posed, edges are still retained, whereas the prefiltering avoids the detection and pronouncing of artificial edges, which are due to the initial noise.
Weickert [39] improved this method taking into account anisotropic diffusion, where the Perona Malik type diffusion is concentrated in the gradient direction of a prefiltered image and a constant diffusion coefficient is considered in the tangent plane. This leads to an additional tangential smoothing along edges and enables to amplify intensity correlations along lines or on level sets. The geometry of this evolution problem especially influences our investigations on anisotropic diffusion, which can be regarded as a further refinement of Weickert's approach. Carmona and Zhong [5] have presented an anisotropic filtering approach that alters the directions of smoothing. They consider Perona-Malik type diffusion in feature directions, and linear diffusion orthogonal to them. Similar to the approach we present here, they define a feature direction to be the eigenvector of the Hessian corresponding to the larger eigenvalue.

In [28] anisotropic diffusion was taken up for the construction of streamline type patterns in flow fields. Concerning the numerical implementation Weickert proposed finite difference schemes [39] and Kačur and Mikula [18] suggested a semi-implicit finite element implementation for the isotropic model by Catté et al.[6]. Adaptive finite element methods in image processing are discussed by Bänsch and Mikula [3], Schnörr [32] and in [29]. Kimmel [20] generalizes scale space methodology to textures on surfaces, considering the appropriate intrinsic differential operators.

Unfortunately, none of the above models is invariant under gray value transformations. An evolution is said to be invariant under gray value transformations, if

$$E(t)(h \circ \phi) = h \circ (E(t)\phi)$$

for mappings $h : \mathbb{R} \to \mathbb{R}$. In the axiomatic work by Alvarez et al. [1] general nonlinear evolution problems were derived from a set of axioms. Especially including the axiom of

gray value invariance they end up with a curvature evolution model, i. e.

$$\partial_t \phi - \|\nabla \phi\| \left(t \operatorname{div} \left(\frac{\nabla \phi}{\|\nabla \phi\|} \right) \right)^{\frac{1}{3}} = 0 \,.$$

Curvature motion has been studied for a long time in geometry and in physics, where interfaces are driven by surface tension. The basic model is the evolution of surfaces by mean curvature, i.e. $\partial_t x = -H(x)N(x)$ where $H(x)$ is the corresponding mean curvature (here defined as the sum of the two principal curvatures), and $N(x)$ is the normal on the surface $\mathcal{M}$ at point x. From differential geometry [14] we know that the mean-curvature vector HN equals the Laplace Beltrami operator applied to the identity $x = \mathrm{Id}$ on a surface $\mathcal{M}$: $H(x)N(x) = -\Delta_{\mathcal{M}} x$. Thus geometric diffusion

$$\partial_t x - \Delta_{\mathcal{M}} x = 0$$

is equivalent to mean curvature motion (MCM). Dziuk [15] presented a semi implicit finite element scheme for MCM on triangulated surfaces. In dimensions higher than two, singularities may occur in the evolution. Generalized, so called viscosity solutions, can be defined in terms of a level set formulation

$$\partial_t \phi - \|\nabla \phi\| \operatorname{div} \left(\frac{\nabla \phi}{\|\nabla \phi\|} \right) = 0 \,.$$

Existence in this context has been proved independently by Evans and Spruck [16] and Chen et al. [8]. The mean curvature H is known to be the first variation of the surface area $\int_{\mathcal{M}} \mathrm{d}x$. We obtain for the area $\mathrm{Ar}(\omega(t))$ of a subset $\omega(t)$ of a smooth surface $\mathcal{M}$ undergoing the MCM evolution (cf. [17]) $\frac{d}{dt}\mathrm{Ar}(\omega(t)) = -\int_{\omega(t)} H^2 \,\mathrm{d}x$. This is one indication for the strong regularizing effect of MCM.

In the context of Finsler geometry we consider for a 1-homogeneous convex scalar function $\gamma(\cdot)$ a generalized weighted area $\int_{\mathcal{M}} \gamma(N) \,\mathrm{d}x$ depending on the surface orientation. As its first variation we obtain the weighted mean curvature H_γ. The corresponding anisotropic curvature flow has been studied for instance by Bellettini and Paolini [4]. In case of plane curves Mikula and Kačur [24] considered an evolution equation for the curvature, from which one can recover the shape of the curves. Concerning the application this is closely related to the preferability of certain interface orientations in the crystalline structure of material (cf. [2, 36]). Deckelnick and Dziuk [11, 12] have analyzed a corresponding fully discrete finite element method and proved convergence toward viscosity solutions.

Concerning the image processing application MCM not only decreases the "geometric" noise but also smooths out geometric features such as edges and corners on the surface. Nevertheless curvature motion terms proved to be successful ingredients in segmentation and image enhancement methods. They have been considered e. g. by Pauwels et al. [26]. Sapiro [30] proposed a modification of MCM considering a diffusion coefficient which depends on the image gradient. Malladi and Sethian [23] presented a numerical level set method on 2D images called "min/max" flow which also considers the curvature evolution, but differing between the smoothing of locally "concave" perturbations on convex shapes and locally "convex" perturbations on concave shapes. We seek another curvature evolution model which overcomes the above mentioned drawback and nicely works on 3D images as well. Our model presented here is based on anisotropic diffusion. As already mentioned the anisotropy will depend on a regularized shape operator and not like in the above anisotropic curvature flow on the normal direction. We emphasize this difference denoting the new model simply *anisotropic geometric diffusion*. On parametric surfaces such a model has already been presented in [10] (cf. Section 4).

3. Some useful geometric tools. While introducing and discussing our method and comparing it to a corresponding model on parametrized surfaces we will make extensive use of some fundamental notion from differential geometry. For a detailed introduction to geometry and differential calculus we refer to [14] and [7, Chapter 1]. Let us consider a smooth compact embedded manifold $\mathcal{M} \subset \mathbb{R}^3$ without boundary. Let $x : \Omega \to \mathcal{M}\,; \xi \mapsto x(\xi)$ be some coordinate map from an atlas. In a sloppy but useful interpretation, we assume that x is also the identity on the embedded surface $\mathcal{M}$. For each point x on $\mathcal{M}$ a tangent space $\mathcal{T}_x\mathcal{M}$ is spanned by the basis $\{\frac{\partial}{\partial\xi_1}, \frac{\partial}{\partial\xi_2}\}$. Due to the embedding in $\mathbb{R}^3$ we identify $\frac{\partial}{\partial\xi_i}$ with the tangent vector $\frac{\partial x}{\partial\xi_i}$. By $\mathcal{T}\mathcal{M}$ we denote the tangent bundle. Measuring length on $\mathcal{M}$ requires the definition of a metric

$$g(\cdot,\cdot) : \mathcal{T}_x\mathcal{M} \times \mathcal{T}_x\mathcal{M} \to \mathbb{R} \qquad \text{with} \qquad g_{ij} = \frac{\partial x}{\partial\xi_i} \cdot \frac{\partial x}{\partial\xi_j}$$

in matrix notation ($g = (g_{ij})_{ij}$), where $\cdot$ indicates the scalar product in $\mathbb{R}^3$. The inverse of g is denoted by $g^{-1} = (g^{ij})_{ij}$. The gradient $\nabla_{\mathcal{M}} f$ of a function f is defined as the representation of df with respect to the metric g. In coordinates we obtain

$$\nabla_{\mathcal{M}} f = \sum_{i,j} g^{ij} \frac{\partial(f \circ x)}{\partial\xi_j} \frac{\partial}{\partial\xi_i}\,.$$

We define the divergence $\mathrm{div}_{\mathcal{M}} v$ for a vector field $v \in \mathcal{T}\mathcal{M}$ as the dual operator of the gradient with respect to the L^2 product on $\mathcal{M}$ and obtain in coordinates

$$\mathrm{div}_{\mathcal{M}} v := \sum_i \frac{\partial}{\partial\xi_i}(v_i\sqrt{\det g})\frac{1}{\sqrt{\det g}}\,.$$

Finally, the Laplace Beltrami operator $\Delta_{\mathcal{M}}$ is given by $\Delta_{\mathcal{M}} u := \mathrm{div}_{\mathcal{M}} \nabla_{\mathcal{M}} u$. Furthermore, we have to consider some fundamental curvature quantities. Let us assume that $\mathcal{M}$ is orientable; then we have a well defined normal $N : \mathcal{M} \to S^2 \subset \mathbb{R}^3$ on $\mathcal{M}$. The second fundamental form $h : \mathcal{T}_x\mathcal{M} \times \mathcal{T}_x\mathcal{M} \to \mathbb{R}$ is locally given by the matrix $h = (h_{ij})_{ij}$ with

$$h_{ij} = h\left(\frac{\partial}{\partial\xi_i}, \frac{\partial}{\partial\xi_j}\right) := -N \cdot x_{,ij} = N_{,i} \cdot x_{,j}.$$

For this symmetric bilinear form we consider the shape operator $S_{\mathcal{T}_x\mathcal{M}}$ defined as the endomorphism on the tangent space $\mathcal{T}_x\mathcal{M}$ with $g(S_{\mathcal{T}_x\mathcal{M}} v, w) = h(v, w)$. It is again symmetric, but now with respect to the metric. In matrix notation we obtain

$$(S_{\mathcal{T}_x\mathcal{M}})_{ij} = \sum_k g^{ik} h_{kj}\,.$$

The eigenvalues κ^j of $S_{\mathcal{T}_x\mathcal{M}}$ are called principal curvatures and the eigenvectors v^j are the principal directions of curvature. Finally we define the *mean-curvature* $H := \mathrm{tr}\, S$. Note that throughout this paper the mean-curvature H is only the sum of the principal curvatures.

4. A parametric model revisited. In this section we will review a first anisotropic diffusion model on parametric surfaces. The general procedure has significant impact on the model to be described in this paper and in a subsequent section we will give a detailed comparison. Smoothing a noisy signal u_0 is usually being done applying a low pass filter, in the most simplest case a Gaussian filter. It is well known that the application of this filter with width σ is equivalent to the evaluation of the heat equation evolution $\partial_t u(t) - \Delta u(t) = 0$

for the signal as initial data $u(0) = u_0$ at time $\frac{\sigma^2}{2}$. In case of noisy parametrized surfaces $\mathcal{M}_0$ with parametrization x_0 we can proceed analogously and consider the corresponding geometric evolution problem. I. e., we seek an one-parameter family of embedded manifolds $\{\mathcal{M}(t)\}_{t\geq 0}$ and corresponding parametrizations $x(t)$, which obey the motion by mean curvature (MCM). For the sake of simplicity we define $MCM(\mathcal{M}_0, t) := \mathcal{M}(t)$, where $\mathcal{M}(t)$ is the solution surface at time t. Thus $MCM(\mathcal{M}, \sigma^2/2)$ can be regarded as the application of a "geometric" Gaussian filter of width σ to $\mathcal{M}$.

Processing of detailed typically noisy or disturbed triangulated surfaces is an important topic in surface modeling and computer graphics. A variety of models has been presented in the literature [13, 21, 22, 35]. In terms of mathematical modeling they can be compared to discrete variants of the basic continuous surface evolution problems of second or fourth order for the parametrization x

$$\partial_t x(t) - \Delta_{\mathcal{M}(t)} x(t) = 0, \qquad \partial_t x(t) + \Delta_{\mathcal{M}(t)} \Delta_{\mathcal{M}(t)} x(t) = 0.$$

Unfortunately, these models do not preserve singular features such

as corners and edges nor do they distinguish directions on the surface. In [10] a novel anisotropic geometric diffusion method was introduced which is able to *preserve important features such as edges and corners* on the surface and which allows tangential smoothing along an edge but not perpendicular to it. The core of the method is a geometric formulation of anisotropic scale space evolution for surfaces. On images, gradients are suitable edge indicators. But the gradient of a coordinate mapping is no intrinsic object on manifolds. The canonical quantity is the shape operator, that indicates edges and corners by sufficiently large eigenvalues. The eigenvector corresponding to a single large eigenvalue is supposed to be orthogonal to the direction of an edge.

Because the evaluation of the shape operator on a noisy surface might be misleading with respect to the original but unknown surface and its edges, we prefilter the current surface $\mathcal{M}(t)$ by straightforward "geometric Gaussian" filtering. Hence, we compute a shape operator $S^\sigma_{\mathcal{T}_x\mathcal{M}}$ on the resulting prefiltered surface $\mathcal{M}_\sigma(t)$, where σ is the corresponding filter width. Finally one obtains the following type of evolution problem

$$\partial_t x - \operatorname{div}_{\mathcal{M}(t)}(a^\sigma_{\mathcal{T}_x\mathcal{M}} \nabla_{\mathcal{M}(t)} x) = r.$$

The diffusion tensor $a^\sigma_{\mathcal{T}_x\mathcal{M}} = a(S^\sigma_{\mathcal{T}_x\mathcal{M}})$ is defined with respect to the orthonormal basis of principal curvature directions on $\mathcal{M}_\sigma$ by

$$a^\sigma_{\mathcal{T}_x\mathcal{M}} = \begin{pmatrix} G(\kappa^{1,\sigma}) & 0 \\ 0 & G(\kappa^{2,\sigma}) \end{pmatrix}$$

where G is a monotone decreasing function with asymptotic limit 0 at ∞ (cf. Section 4). Thus, diffusion on the surface is significantly reduced in directions of high principal curvature, i. e. those perpendicular to an edge. On the other hand, a larger diffusion coefficient in the edge direction enables tangential smoothing along the edge. The right hand side r of the considered evolution problem can be chosen such that the volume enclosed by $\mathcal{M}$ is preserved (cf. [10]) or one can select a simple retrieving force which avoids large deformations. Motivated by our definition of the diffusion tensor $a^\sigma_{\mathcal{T}_x\mathcal{M}}$ we define a generalized $a^\sigma_{\mathcal{T}_x\mathcal{M}}$-mean curvature

$$H_{a^\sigma_{\mathcal{T}_x\mathcal{M}}} := \operatorname{tr}(a^\sigma_{\mathcal{T}_x\mathcal{M}} \circ S_{\mathcal{T}_x\mathcal{M}})$$

which turns out to be the negative propagation speed of our model in normal direction. Figure 4.1 shows results of this approach.

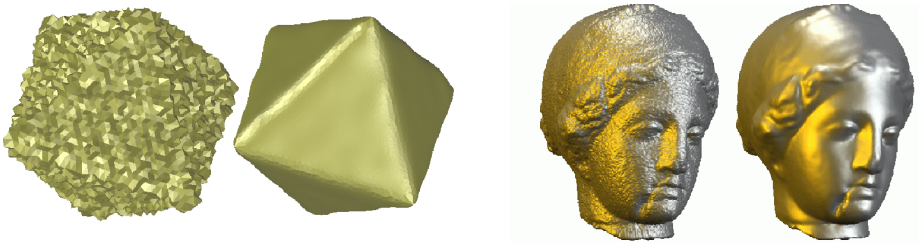

FIG. 4.1. Two different noisy initial triangulated surfaces (first and third picture) are evolved under the parametric anisotropic geometric evolution. Smoothed representations extracted at suitable scales from the evolution are depicted (second and fourth picture) (cf.[10]).

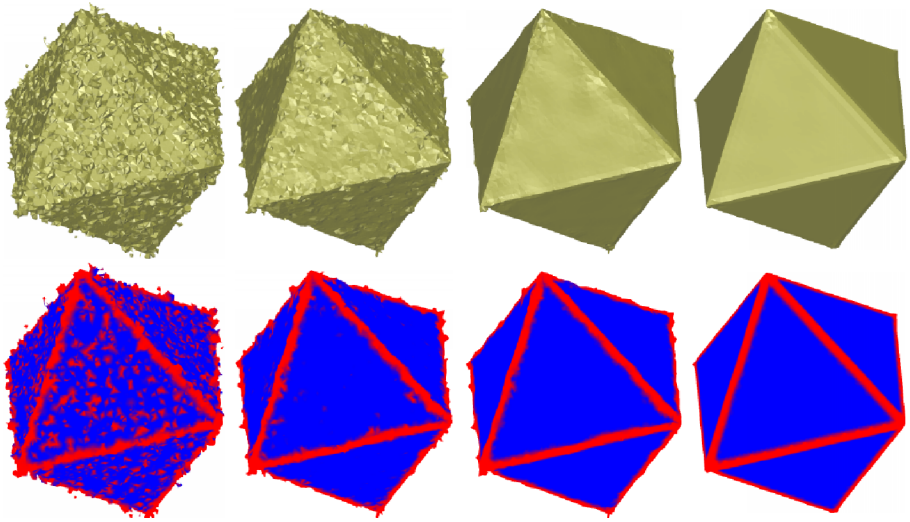

FIG. 5.1. As a test case we consider the function $\phi(x) = |x_1| + |x_2| + |x_3|$ whose level sets are octahedrons. This function was perturbed and then taken as initial data for the anisotropic geometric diffusion method. From left to right an original perturbed level set and the corresponding first, second, and fifth time step of its evolution on a 64^3 grid are depicted. In the lower row we visualize the dominant curvature on the level sets from the upper row. A color ramp from blue to red indicates the dominant curvature value.

5. Anisotropic geometric diffusion on level sets. On the background of the previous expositions we are now prepared to discuss an anisotropic geometric diffusion approach as a suitable morphological scale space method in 3D image processing. We will define a level set formulation for a generalized anisotropic curvature motion of the isosurfaces. Thus, we simultaneously deal with all level sets, although in certain applications our interest is focused on one specific implicit surface, possibly in advance converted from a parametric to an implicit representation. The similarities and especially the peculiar differences to the parametric model (cf. Section 4) will be discussed in detail in Section 9. First, we outline the basic ingredients and the general procedure:

• Let us denote by $\phi_0 : \Omega \to \mathbb{R}$ the gray value function of the initial 3D image with inscribed level sets

$$\mathcal{M}_0^c := \{x \in \Omega \,|\, \phi_0(x) = c\}\,.$$

We assume ϕ_0 and the set of corresponding implicit surfaces $\{\mathcal{M}_0^c\}_c$ to be noisy and ask for a family of successively smoothed images $\{\phi(t,\cdot) \,|\, t \in \mathbb{R}_0^+\}$ where $\phi(t,\cdot) : \Omega \to \mathbb{R}$

and $\phi(0,\cdot) = \phi_0(\cdot)$. Throughout this paper Ω will always be the unit cube $[0,1]^3$. As common in multiscale calculus on images and surfaces the time t serves as the scale parameter. Thereby, for each gray value c a family of surfaces $\{\mathcal{M}^c(t)\}_{t\in\mathbb{R}_0^+}$ is generated, with $\mathcal{M}^c(0) = \mathcal{M}_0^c$. Here, as long as we derive the model we assume $\phi(\cdot,\cdot)$ to be sufficiently smooth and $\nabla\phi(t,x) \neq 0$ for all $(t,x) \in \mathbb{R}_0^+ \times \Omega$. Indeed, due to the implicit function theorem the corresponding sets $\mathcal{M}^c(t)$ then are actually smooth surfaces.

The method should be invariant under gray scale transformations. To ensure this purely morphological character we confine to curvature quantities as the driving forces for the corresponding evolution of the level sets. The simplest morphological smoothing model would be to consider mean curvature motion of the level sets (cf. Section 2).

• But in addition to the smoothing of the level sets our aim is to maintain or even enhance edges on these surfaces. As already described in Section 4 an edge feature is characterized by a small curvature in tangential direction along the feature and a sufficiently large curvature in the perpendicular direction in the tangent space. In case of embedded surfaces the corresponding curvature tensor is represented by the shape operator $S_{\mathcal{T}_x\mathcal{M}}$. In the vicinity of an edge there will be a small and a large eigenvalue κ^1 and κ^2 respectively. The corresponding eigenvectors v^1 and v^2 indeed point in tangential direction along the edge and in the orthogonal direction respectively (cf. Section 4). Hence, we consider an anisotropic diffusion tensor depending on the extended shape operator S, which significantly decreases the diffusion coefficient in the dominant curvature direction v^2, whereas a fixed diffusion coefficient is prescribed in the sub-dominant v^1 direction. This distinction will again be made via a function G applied to the principle curvatures κ^1, κ^2. Fig. 5.1 illustrates the method's performance for a test case of a perturbed 3D image with originally sharp edges and shows time steps of the evolution. The choice of G is related to the selection of the diffusion coefficient in the Perona Malik model [27].

• The evaluation of the shape operator on a level set of a noisy image might be misleading with respect to the true but unknown level sets and edges. E. g. noise might be identified as features. Therefore we have to consider a regularization in advance and prefilter the current image $\phi(t,\cdot)$ before evaluating the shape operator. Here we have the choice to either globally or locally regularize the image. An appropriate "morphological" filter — a short time-step of a level set evolution by mean curvature — would deliver a global regularization. As a simple alternative we can consider the convolution of $\phi(t,\cdot)$ with some kernel with compact support. However, concerning an implementation on discrete data these two global regularization approaches still require the definition of a shape operator. This involves second derivatives on a typical representation of image data by piecewise trilinear functions. On the other hand we can take into account a local projection of the image intensity on a suitable finite dimensional space of smooth functions. Then, on this regularization we do not encounter the problem of a definition of the shape operator and its evaluation is straight forward. In Section 6 we will analyze the different regularization methods in detail.

We end up with the following type of nonlinear parabolic problem. Given an initial 3D image ϕ_0 on a domain Ω, we ask for a scale of images $\{\phi(t,\cdot)\}_{t\geq 0}$ which obey the anisotropic geometric evolution equation:

$$\partial_t\phi - \|\nabla\phi\| \operatorname{div}\left(a^\sigma \frac{\nabla\phi}{\|\nabla\phi\|}\right) = 0 \tag{5.1}$$

on $\mathbb{R}^+ \times \Omega$ and satisfy the initial condition $\phi(0,\cdot) = \phi_0(\cdot)$. Furthermore, we suppose natural boundary conditions on $\partial\Omega$, i. e.

$$a^\sigma \frac{\partial\phi}{\partial\nu} = 0$$

where ν denotes the outer normal on $\partial\Omega$. The diffusion tensor a^σ is supposed to be a symmetric, positive semidefinite endomorphism on $\mathbb{R}^3$, which cares about the preservation of edges and the tangential smoothing along edges.

Now, our main objective is the appropriate concrete choice of the anisotropy at some point $x \in \mathcal{M} := \mathcal{M}^c(t)$ ($\phi(t,x) = c$). Therefore, let us first examine the Jacobian of the normal $N := \frac{\nabla\phi}{\|\nabla\phi\|}$. We define

$$S := DN = (N_{i,j})_{i,j} = \frac{1}{\|\nabla\phi\|}(\mathrm{Id} - N \otimes N)D^2\phi.$$

This mapping S can be regarded as an extension to $\mathbb{R}^3$ of the shape operator $S_{\mathcal{T}_x\mathcal{M}}$ on $\mathcal{T}_x\mathcal{M}$. Obviously, from $DN \cdot N = 0$ it follows that the restriction $S(\mathrm{Id} - N \otimes N)$ is a symmetric mapping from $\mathcal{T}_x\mathcal{M}$ onto $\mathcal{T}_x\mathcal{M}$. It actually conincides on $\mathcal{T}_x\mathcal{M}$ with the Shape Operator $S_{\mathcal{T}_x\mathcal{M}}$. Thus, S is characterized by the eigenvalues κ^1, κ^2, 0 and the eigenvectors v^1, v^2 and N. Therefore, we will denote S the extended shape operator. Now we define the anisotropic diffusion tensor a^σ as a function of a regularized shape operator S^σ based on an at least locally regularized surface $\mathcal{M}_\sigma$

$$a^\sigma := \mathcal{A}(S^\sigma)$$

where $\mathcal{A} : \mathbb{R}^{3\times3} \to \mathbb{R}^{3\times3}$. As a suitable choice for this mapping $\mathcal{A}$ we consider the scalar function G from the basic image processing model, with $G(s) = (1 + \lambda^{-2}s^2)^{-1}$, now acting on the space of symmetric maps $\mathrm{Sym}(\mathcal{T}_x\mathcal{M})$. Mapping the normal space to the 0 we trivially expand it to $\mathrm{Sym}(\mathbb{R}^3)$. Here λ serves as a steering parameter for the identification of edges. For larger value λ more features on the surface will be regarded as edges and preserved by the proposed diffusion method. In our applications we always choose $\lambda = 0.3$. Let us recall, that in image processing by the Perona Malik model λ is exactly the switch between backward and forward diffusion. We suppose $S^\sigma(\mathrm{Id} - N \otimes N)$ to diagonalize with respect to the basis $\{v^{1,\sigma}, v^{2,\sigma}\}$, where $v^{1,\sigma}, v^{2,\sigma}$ are eigenvectors corresponding to principal curvatures $\kappa^{1,\sigma}, \kappa^{2,\sigma}$ on $\mathcal{M}_\sigma$ and N^σ is the normal. Hence we obtain the matrix representation

$$\mathcal{A}(S^\sigma) = B_\sigma^T \begin{pmatrix} G(\kappa^{1,\sigma}) & & \\ & G(\kappa^{2,\sigma}) & \\ & & 0 \end{pmatrix} B_\sigma \,.$$

Here $B_\sigma \in SO(3)$ is the basis transformation from the regularized frame of principal directions of curvature and the normal $\{v^{1,\sigma}, v^{2,\sigma}, N^\sigma\}$ onto the canonical basis $\{e_1, e_2, e_3\}$, where $N^\sigma \perp v^{i,\sigma}$.

Figure 5.2 picks up the initial example for the introduction (cf. Fig. 1.1). A 3D echocardiographical image of a human heart is taken as initial data. Here, different time steps of the evolution under anisotropic geometric diffusion are shown. A second and third example is concerned with true measurement data. The salt concentration in a density driven flow through a porous medium filled with fresh and salt water is measured in a laboratory experiment by an MRI device. In Figure 5.3 level sets of the salt concentration are drawn, whereas Figure 5.4 shows slices through the 3D data set at different stages of the experiment. In both cases we compare the original measurement data with smoothed results obtained by our method. Below we will furthermore be concerned with volume conservation especially tested on this data set. Figures 5.5 and 5.6 show smoothing results via the anisotropic geometric diffusion method in case of a fingering experiment, where heavy salt water is entering on top of a basin filled with lighter fresh water. The salt water is pulled downwards due to gravity. The underlying instability in this configuration leads to a fingering effect on the interface between fresh and salt water.

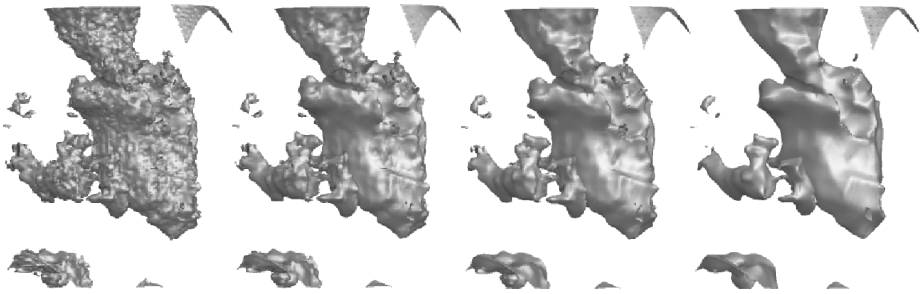

FIG. 5.2. From left to right a certain level set - visualizing the shape of one ventricle of the human heart - is extracted from the anisotropic geometric evolution. Here successive successive steps of the smoothing process are shown (cf. Fig. 1.1). The computation was performed on a 128^3 grid.

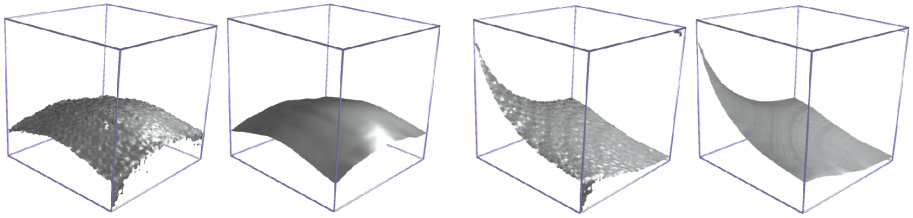

FIG. 5.3. The application of the anisotropic geometric level set method to experimental data from a fresh and salt water experiment is depicted. In the first and third image isolevels of a salt-concentration are shown at two different stages of the experiment. First, the salt water is floating into a container filled with fresh water (left). Then an outlet is opened at one of the top corners of the container (right). During the experiment, concentration of the salt was measured using an MR imaging device. The second and fourth image show the corresponding 3D images obtained by anisotropic geometric diffusion on a 64^3 grid (cf. also Fig. 5.4).

Remark: Obviously, independent of the question of wellposedness, it is essential that a^σ depends on the regularized S^σ and not on the actual shape operator S. Otherwise we would obtain a trivial evolution problem, which rests at the initial image. Indeed from $\ker \mathcal{A}(S) = \mathrm{span}\{N\}$ we get $\mathcal{A}(S)N = 0$.

Remark: Already mean curvature motion in level set formulations leads to a degenerate parabolic problem, where diffusion is restricted to the tangent space. Considering the regularized level set $\mathcal{M}_\sigma$ in our model we immediately observe that the resulting tangent space $\mathcal{T}_x\mathcal{M}_\sigma$ no longer coincides with the actual tangent space $\mathcal{T}_x\mathcal{M}$. Thus, in case of very noisy data it can not be guaranteed that $\mathcal{A}(S^\sigma)$ still acts as a positive definite endomorphism on $\mathcal{T}_x\mathcal{M}$. In fact, N^σ might be contained in $\mathcal{T}_x\mathcal{M}$. Positive definiteness can be enforced introducing a small, positive diffusion coefficient α in the direction of N^σ as well. Hence, we obtain

$$a^\sigma := \mathcal{A}^\alpha(S^\sigma)\,.$$

where $\mathcal{A}^\alpha(S^\sigma) = \mathrm{diag}(G(\kappa^{1,\sigma}), G(\kappa^{2,\sigma}), \alpha)$ with respect to the basis $\{v^{1,\sigma}, v^{2,\sigma}, N^\sigma\}$. In our applications we observed no problems with the latter type of degeneracy and confine to the original model with $\alpha = 0$.

In what follows, we will more closely examine the geometry of the proposed method. The underlying evolution turns out to be equivalent to the propagation of the level sets $\mathcal{M}^c(t)$ with speed f in normal direction N, i. e. $\partial_t x = f\,N$ holds for

$$f := \mathrm{tr}(a^\sigma(S_\sigma - S)) + (\mathrm{div}\, a^\sigma)(N^\sigma - N)\,.$$

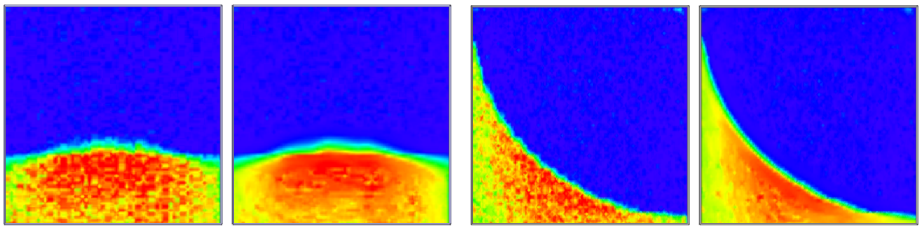

FIG. 5.4. From the development of the concentration distribution in the experimental data (cf. Fig. 5.3) vertical slices are extracted. Again in the first and the third image the actual measurements are visualized at the two different stages of the experiment, whereas in the second and fourth picture the corresponding slices through the smoothed data sets are shown.

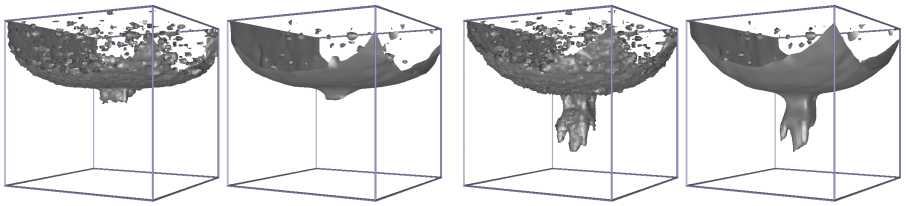

FIG. 5.5. The anisotropic geometric level set method is applied to noisy data from a fingering experiment in a two phase porous medium flow of fresh and salt water. During the experiment the salt concentration was measured using an MR imaging device. On the left isosurfaces of the salt concentration at an early time in the experiment are shown, whereas the right images show data from a later time in the experiment. The first and the third image represent the original data. In the second and fourth image the 3D data obtained by the anisotropic diffusion on a 64^3 grid are shown (cf. also Fig. 5.6).

Here we define $S_\sigma = DN^\sigma$. Let us emphasize that S_σ coincides with the actually considered regularized shape operator S^σ, if we evaluate the latter on level sets of a globally prefiltered image. Evaluating S^σ separately for each point $x \in \Omega$ on a locally regularized surface $\mathcal{M}_\sigma$ we in general obtain $S^\sigma \neq S_\sigma$.

Proof. Picking up the above notation for the anisotropy, the normal vectors N,N^σ on $\mathcal{M}$, $\mathcal{M}^\sigma$, respectively, we obtain

$$\begin{aligned}
\operatorname{div}(a^\sigma N) &= (\operatorname{div} a^\sigma)N + \operatorname{tr}(a^\sigma DN) \\
&= (\operatorname{div} a^\sigma)N^\sigma + (\operatorname{div} a^\sigma)(N - N^\sigma) + \operatorname{tr}(a^\sigma S) \\
&= \operatorname{div}(a^\sigma N^\sigma) - \operatorname{tr}(a^\sigma DN^\sigma) + (\operatorname{div} a^\sigma)(N - N^\sigma) + \operatorname{tr}(a^\sigma S) \\
&= 0 - \operatorname{tr}(a^\sigma S_\sigma) + (\operatorname{div} a^\sigma)(N - N^\sigma) + \operatorname{tr}(a^\sigma S)\,.
\end{aligned}$$

Therefore, our problem can be rewritten as

$$\partial_t \phi + \|\nabla\phi\| \left(\operatorname{tr}(a^\sigma (S_\sigma - S)) + \operatorname{div} a^\sigma (N^\sigma - N)\right) = 0\,.$$

Due to the equivalence of the level set equation $\partial_t \phi + \|\nabla\phi\| f = 0$ and the corresponding parametric evolution $\partial_t x = f N$ we have verified our claim. □

The evaluation of the shape operator is based on second order derivatives, whereas the normal only relies on first order derivatives. Thus, for noisy images we expect

$$\|S_\sigma(x) - S(x)\| \gg \|N(x) - N^\sigma(x)\|$$

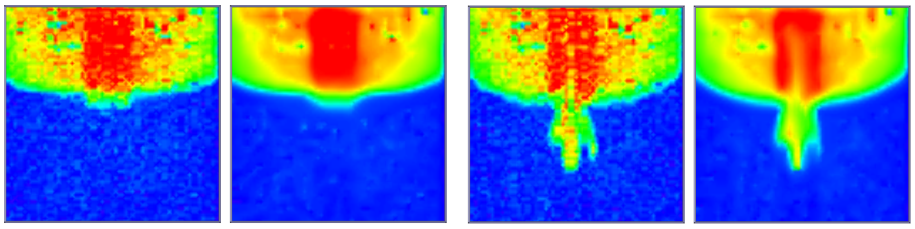

FIG. 5.6. From the experimental data shown in Figure 5.5 vertical slices are extracted. Again two successive stages of the experiment are depicted. The first and the third image show slices through the original data; corresponding slices through the smoothed data sets are shown in the second and fourth image.

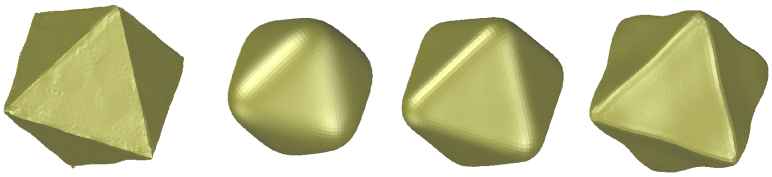

FIG. 5.7. We compare the principle, qualitative behavior of different methods extracting level sets at a relatively large time in the evolution: anisotropic geometric diffusion (left), mean curvature motion (middle left), isotropic Perona Malik diffusion [27] (middle right), and anisotropic diffusion model proposed by Weickert [38] (right). Always the same time step $t = 0.00375$ is depicted from the corresponding evolution. The computations were performed on a 64^3 grid and the build in regularization was balanced with respect to an equivalence of a filter width $\sigma = 4\,h$. Thus, for the isotropic and anisotropic diffusion models (right) we regularized by a time step $\sigma^2/2$ of the heat equation. Finally, for the anisotropic geometric diffusion we took $l = 4$.

for general points $x \in \Omega$. Therefore, $\mathrm{tr}(a^\sigma(S_\sigma - S))$ will be the dominant term in the propagation speed in normal direction. Finally, this allows us to give a nice geometric interpretation of the proposed evolution problem:

> *The anisotropic level set evolution is mainly driven by the difference of a regularized shape operator and the true shape operator weighted applying the anisotropic weights given by the diffusion tensor.*

Furthermore, we verify that the propagation speed f vanishes, if $N^\sigma \equiv N$ (cf. Section 9). Besides the morphological character of the proposed approach especially this built-in comparison between regularized and actual shape operator and normal gives reason for the method's performance. Figure 5.7 compares different evolution methods in image processing. We have balanced parameters and consider a rather long time in the evolution. For none of the methods this reflects a proper choice of parameters and time but it strongly reflects their principle behavior.

In general we can not guarantee that $\nabla\phi \neq 0$ even if the initial data fulfills this regularity assumptions. In fact, Evans and Spruck [16] gave an example for mean curvature motion by the level set approach where a certain level set degenerates and the corresponding $\mathcal{M}^c(t)$ fattens, loosing its surface property. Thus, we have to regularize the problem replacing the norm $\|\cdot\|$ in equation (5.1) by a regular approximation $\|\cdot\|_\epsilon$. I. e. we choose (cf. [16])

$$\|v\|_\epsilon = \sqrt{\epsilon^2 + \|v\|^2}\,.$$

The corresponding regularized variational formulation is then given by

$$\left(\frac{\partial_t\phi}{\|\nabla\phi\|_\epsilon}, \vartheta\right) + \left(\mathcal{A}(S^\sigma)\,\frac{\nabla\phi}{\|\nabla\phi\|_\epsilon}, \nabla\vartheta\right) = 0\,, \tag{5.2}$$

for all test functions $\vartheta \in C^\infty(\Omega)$. Here $(\cdot,\cdot)$ indicates the L^2 product on Ω. Considering a finite element implementation we will pick up this formulation in Section 7.

6. A regularized shape operator. In our model above we have made extensive use of a regularized shape operator S^σ, on which we base the computation of the anisotropic diffusion tensor. As already described in the previous Section 5 we have different choices for the definition of the regularization:

1. The geometrically natural and purely morphological presmoothing of an image is given by a *short time evolution under mean curvature motion.* Thus, for every $t \in \mathbb{R}_0^+$ we may solve

$$\partial_t \psi - \|\nabla\psi\| \operatorname{div}\left(\frac{\nabla\psi}{\|\nabla\psi\|}\right) = 0$$

with initial data $\psi(0,\cdot) = \phi(t,\cdot)$ and natural boundary conditions and evaluate the shape operator $S^\sigma(x) = S(\phi^\sigma, x)$ on $\phi^\sigma(t,\cdot) := \psi(\frac{\sigma^2}{2},\cdot)$. The advantage of this approach is that the resulting model is completely defined in morphological terms only.

2. Another simpler — but not morphological — approach is the regularization via *convolution* of the image with a kernel K_σ of width σ, i.e. $\phi^\sigma := K_\sigma * \phi$, and again the definition $S^\sigma(x) = S(\phi^\sigma, x)$.

3. As already mentioned with respect to a discretization, we are still left to define a discrete shape operator on level sets described by a finite element function. As long as we do not use at least quadratic elements even a suitable definition — without taking into account the consistency problem — remains an open question [31]. Since typically images are discretized based on trilinear interpolation of pixel or voxel values, our method of choice is one based on local regularization. Unfortunately the local regularization defined in the sequel is not guaranteed to be invariant under gray value transformations. Nevertheless we expect the corresponding regularized shape operator to depend essentially only on the morphology of the local image. We base the local regularization on a least squares fit — in fact *local L^2 projection* — of the image ϕ onto a subspace of the space of quadratic polynomials $\mathcal{P}_2$. To this end let us fix a point $x \in \Omega$ and denote by $\mathcal{Q} := \operatorname{span}\{x_1^2, x_2^2, x_3^2,\ x_1x_2, x_1x_3, x_2x_3,\ x_1, x_2, x_3\}$ this subspace of $\mathcal{P}_2$. We skip the constant functions in $\mathcal{Q}$, since we assume the image ϕ to be locally shifted such that $\phi(x) = 0$. The local L^2 projection $\Pi_{x,\sigma}\phi \in \mathcal{Q}$ of the intensity ϕ onto $\mathcal{Q}$ is then defined via the orthogonality relation

$$\int_{\mathcal{B}_\sigma(x)} (\phi(y) - (\Pi_{x,\sigma}\phi)(y))\ q\ dy = 0 \qquad \forall\, q \in \mathcal{Q},$$

where $\mathcal{B}_\sigma(x)$ is a small neighborhood of x (cf. Fig. 6.1 for the effect of different stencil width parameter σ on the evolution result). For the ease of presentation we write $\phi_x^\sigma(y)$ instead of $(\Pi_{x,\sigma}\phi)(y)$ for a fixed $x \in \Omega$. Locally, the projection defines a surface $\mathcal{M}_\sigma^x$, whose tangent space $\mathcal{T}_y\mathcal{M}_\sigma^x$ in general does not coincide with $\mathcal{T}_x\mathcal{M}$ because in general $N_x^\sigma(y) := \frac{\nabla\phi_x^\sigma(y)}{\|\nabla\phi_x^\sigma(y)\|} \neq N$.

Now we define in analogy to the non-regularized case the shape operator $S^\sigma = S(\phi_x^\sigma(y)) := D_y N_x^\sigma(y)$, whose restriction $S^\sigma(\mathrm{Id} - N^\sigma \otimes N^\sigma)$ is again a symmetric mapping from $\mathcal{T}_y\mathcal{M}_\sigma^x$ onto $\mathcal{T}_y\mathcal{M}_\sigma^x$ (cf. Section 5). Thus, $S^\sigma(\mathrm{Id} - N^\sigma \otimes N^\sigma)$ is characterized by its eigenvalues $\kappa^{j,\sigma}$, $j = 1, 2$ and the eigenvectors $\{v^{1,\sigma}, v^{2,\sigma}\}$. Therefore, with an appropriate basis transformation $B_\sigma \in SO(3)$, we obtain

$$S^\sigma(\mathrm{Id} - N \otimes N) = B_\sigma^T \begin{pmatrix} \kappa^{1,\sigma} & & \\ & \kappa^{2,\sigma} & \\ & & 0 \end{pmatrix} B_\sigma.$$

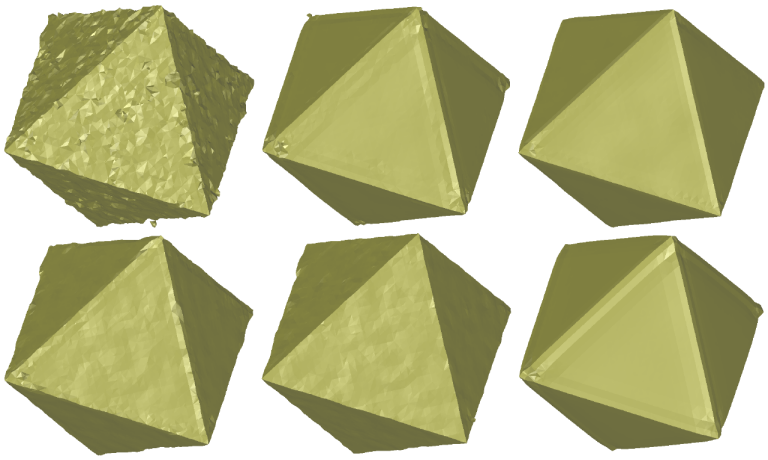

FIG. 6.1. We compare the influence of the filter width parameter σ on the results of the anisotropic curvature evolution. As initial data we consider the noisy octahedron data set already shown in Fig. 5.1 and choose $\sigma = 2\,h$ (left column), $\sigma = 4\,h$ (middle column), and $\sigma = 8\,h$ (right column). The upper row shows the first time step of the evolution whereas in the lower row the third time step of the evolution is shown. The results obviously reflect our theoretical expectations (cf. remark in Section 6).

Let us again emphasize that this $S^\sigma = S(\phi_x^\sigma)$ is evaluated for every x separately and therefore in general $S^\sigma \neq S_\sigma$. Finally we observe that in case of coinciding ϕ_x^σ and ϕ the nonregularized and regularized shape operator and normal are equal, i. e. $S^\sigma = S_\sigma = S$ and $N^\sigma = N$. This especially holds if $\phi \in \mathcal{P}_2$. Thus, quadratic image intensities and induced ellipsoidal shapes are invariant under the proposed anisotropic geometric diffusion.

Remark: Still we have to select a proper regularization parameter σ, which always plays the role of a stencil width, either in a geometric smoothing (regularization variant 1), in a linear convolution (variant 2), or in the actually implemented L^2 projection method (variant 3). As usual in diffusion processes the stopping time t of the geometric diffusion process is related to a filter width $\sqrt{2\,t}$ (cf. Section 4). Thus it is reasonable with respect to the modeling to choose $\sigma \approx \sqrt{2\,t}$ (cf. Morel and Solimini [25]). Due to the trade off between smaller values of σ leading to more detailed feature detection and larger σ values improving the consistency of the extracted shape operator for smooth data we choose $\sigma \approx l\,h$, e. g. $l \approx 4$ in our applications. Independent of the choice of regularization the derived regularized shape operator acts as a quantized indicator for the relevance of edges and their direction and not as a descriptor of the somehow optimal limit shape.

7. Finite element discretization. Up to now we have considered an image intensity ϕ which has been a sufficiently smooth function on the image domain $\Omega \subset \mathbb{R}^3$. Concerning the implementation of the proposed multiscale method and its actual application to digital images we now have to discretize our model in space and time. In the application images typically arise as arrays of pixels. We interpret pixel values as nodal values on a uniform hexahedral mesh $\mathcal{C}$ covering the whole image domain Ω and consider the corresponding trilinear interpolation on cells $C \in \mathcal{C}$ to obtain discrete intensity functions in the accompanying finite element space. To clarify the notation we will always denote spatially discrete quantities with upper case letters to distinguish them from the corresponding continuous quantities in lower case letters. A subscript h indicates the grid size. Let us define the space of piecewise trilinear, continuous functions

$$V^h = \{\Phi \in C^0(\Omega) \,|\, \Phi|_C \in \mathcal{P}_1 \otimes \mathcal{P}_1 \otimes \mathcal{P}_1 \,\forall C \in \mathcal{C}\}\,,$$

where $\mathcal{P}_1$ denotes the space of linear polynomials and "$\otimes$" the tensor product.

Now we are able to formulate our discrete problem. Discretizing first only in space we obtain a variational finite element formulation of our level set evolution problem (cf. Eq. (4.1) for the continuous case):
Find $\Phi : \mathbb{R}_0^+ \to V^h$ *with initial data* $\Phi(0) = \mathcal{I}_h\phi_0$, *such that for all* $\theta \in V^h$

$$\left(\frac{\partial_t \Phi}{\|\nabla\Phi\|_\epsilon}, \theta\right)^h + \left(A^\sigma \frac{\nabla\Phi}{\|\nabla\Phi\|_\epsilon}, \nabla\theta\right) = 0.$$

Here, $\mathcal{I}_h : C^0(\Omega) \to V^h$ is the Lagrange interpolation on the grid $\mathcal{C}$ and the diffusion tensor A^σ is supposed to be a suitable approximation of a^σ. Finally, we have used the lumped mass scalar product $(\cdot,\cdot)^h$, which is defined by

$$(U, V)^h := \sum_{C\in\mathcal{C}} \int_C \mathcal{I}_h(U\,V)\,\mathrm{d}x$$

for discrete functions $U, W \in V^h$ (cf. [37]). As an immediate consequence the corresponding nonlinear mass matrix $M_h(\Phi)$ is diagonal. This simplifies the resulting scheme significantly. We end up with a system of ordinary differential equations for the nodal values of the intensity function Φ. Obviously the regularization parameter ϵ should be coupled somehow with the grid size. Following Dziuk and Deckelnick [12] we select $\epsilon \approx h$.

Next, we have to discretize in time, which includes the choice of some time stepping scheme and the decision which term to handle implicitly and which explicitly. Here we choose a semi-implicit backward Euler discretization. Expressed in geometric terms we consider the metric and the regularized shape operator explicitly (cf. [15]). I. e. the shape operator is updated every time step and we expect and experimentally observe surface features such as edges to be successively better identified via the principle curvature evaluation on S^σ. Let τ be a selected time step size. Then we obtain the time and space discrete problem:

Find a sequence of discrete intensity functions $\{\Phi^n\}_{n=0,\dots}$ *with* $\Phi^n \in V^h$ *and* $\Phi^0 = \mathcal{I}_h\phi_0$, *such that for all* $\theta \in V^h$

$$\left(\frac{1}{\|\nabla\Phi^n\|_\epsilon}\frac{\Phi^{n+1}-\Phi^n}{\tau}, \theta\right)^h + \left(A^\sigma \frac{\nabla\Phi^{n+1}}{\|\nabla\Phi^n\|_\epsilon}, \nabla\theta\right) = 0.$$

We expect Φ^n to be an approximation of $\Phi(n\tau)$. Finally, in each step of the discrete evolution we have to solve a single system of linear equations. In terms of nodal vectors indicated by a bar on top of the corresponding discrete function we can rewrite the scheme and get

$$\left(M_h(\Phi^n) + \tau L_h(\Phi^n)\right)\bar{\Phi}^{n+1} = M_h(\Phi^n)\bar{\Phi}^n \tag{7.1}$$

for the new vector of nodal values $\bar{\Phi}^{n+1}$ at time $t_{n+1} = (n+1)\tau$. Here, we have applied the nonlinear lumped mass and stiffness matrices

$$M_h(\Phi) = \left(\left(\frac{\Psi_i}{\|\nabla\Phi^n\|_\epsilon}, \Psi_j\right)^h\right)_{ij}, \qquad L_h(\Phi) = \left(\left(A_n^\sigma \frac{\nabla\Psi_i}{\|\nabla\Phi^n\|_\epsilon}, \Psi_j\right)\right)_{ij},$$

where $\{\Psi_j\}_j$ is the nodal basis of V^h.

In each time step the discrete diffusion tensor A_n^σ is evaluated for every grid node separately. Then, on cells $C \in \mathcal{C}$ we use trilinear interpolation to define A_n^σ. Furthermore, in the

numerical application we have replaced the integration of $(A_n^\sigma \frac{\nabla \Psi_i}{\|\nabla \Phi^n\|_\epsilon}, \Psi_j)$ by the one point numerical quadrature which refers only to the value at the element's center of mass.

The resulting systems of linear equations, which arise in each time step of the discrete anisotropic curvature evolution are solved by a *preconditioned conjugate gradient method.* For computations on a 128^3 grid the solver typically needs 60 iterations to decrease the relative residual below 10^{-5}.

8. Shape operator on discrete data. In this section we will describe how to compute the local L^2 projection defined in Section 6 on given discrete image data $\Phi \in V^h$. Without loss of generality we will assume that $x = 0$ and furthermore that $\phi(x) = 0$. Since we are working on hierarchical octtree grids, it is natural to define the σ neighborhood $\mathcal{B}_\sigma(x)$ in the maximum norm: For an $l \in \{2m \,|\, m \in \mathbb{N}\}$ we set $\mathcal{B}_\sigma(x)$ to be a patch containing $(l+1) \times (l+1) \times (l+1)$ nodes having x in its center. In other words $\mathcal{B}_\sigma$ consists of $l \times l \times l$ elements. Then for $\sigma = \operatorname{diam} \mathcal{B}_\sigma(x)$, we obtain $\sigma = l\,h$.

To compute the projection $\Phi_x^\sigma(y) := (\Pi_{x,\sigma}\Phi)(y)$ onto the subspace $Q = \operatorname{span}\{x_1^2, x_2^2, x_3^2, x_1x_2, x_1x_3, x_2x_3, x_1, x_2, x_3\}$ of $\mathcal{P}_2$, we consider the representation $\Phi_x^\sigma(y_1, y_2, y_3) := \sum_{i=1}^9 \alpha_i q_i$ in the above canonical basis of $\mathcal{Q}$. Then $(\alpha_i)_i \in \mathbb{R}^9$ solves the linear system of equations

$$\sum_{j=1}^{9} \left(\int_{\mathcal{B}_\sigma(x)} q_i\, q_j \, dy \right) \alpha_j = \int_{\mathcal{B}_\sigma(x)} \Phi\, q_i \, dy$$

for $i = 1, \ldots, 9$. For a fixed l, the inverse of the matrix on the left hand side of the above equation can be precomputed on regular grids. This speeds up the projection process in the implementation considerably. We easily derive that

$$N^\sigma(y)\big|_{y=0} = \frac{1}{\sqrt{\alpha_7^2 + \alpha_8^2 + \alpha_9^2}} \begin{pmatrix} \alpha_7 \\ \alpha_8 \\ \alpha_9 \end{pmatrix}, \qquad D^2\Phi^\sigma(y)\big|_{y=0} = \begin{pmatrix} 2\alpha_1 & \alpha_4 & \alpha_5 \\ \alpha_4 & 2\alpha_2 & \alpha_6 \\ \alpha_5 & \alpha_6 & 2\alpha_3 \end{pmatrix}.$$

Finally, recalling the definition of the regularized shape operator S^σ, we obtain a formula of the shape operator S^σ in terms of the above quantities, i. e.

$$S^\sigma = \frac{1}{\|\nabla \Phi^\sigma\|} \left(D^2\Phi^\sigma - N^\sigma \otimes D^2\Phi^\sigma\, N^\sigma \right).$$

After a restriction of the obtained operator onto the tangent space $\mathcal{T}_y \mathcal{M}_\sigma^x = (N^\sigma)^\perp$, which then results in $S^\sigma(\mathrm{Id} - N^\sigma \otimes N^\sigma)$ we easily can evaluate the principal curvatures $\kappa^{j,\sigma}$ and principal directions of curvature $v^{j,\sigma}$.

To study the consistency of the curvature evaluation we again pick up the second regularization method based on local convolution of the image with a kernel K_σ. We expect our actually applied third regularization method to behave similar concerning the interplay of filter width and grid size. Let us suppose ϕ to be smooth, at least contained in the usual Sobolev space $H^{3,p}$ for $1 \le p < \infty$. If we consider a nodal interpolation Φ in the finite element space, we obtain a second order approximation result [9], i. e. $\|\phi - \Phi\|_{0,p} \le C\,h^2$. Next, we consider the convolution $\Phi^\sigma = K_\sigma * \Phi$ and evaluate second derivatives on Φ^σ as a simplification of the evaluation of curvatures on level sets of Φ^σ. In this case a consistency analysis is straightforward. We estimate

$$\begin{aligned} \left\| D^2(K_\sigma * \Phi) - D^2\phi \right\|_{L^p} &\le \left\| (D^2 K_\sigma) * (\Phi - \phi) \right\|_{L^p} + \left\| K_\sigma * D^2\phi - D^2\phi \right\|_{L^p} \\ &\le C \left(\frac{h^2}{\sigma^2} + \sigma \right) \|\phi\|_{H^{3,p}} \end{aligned}$$

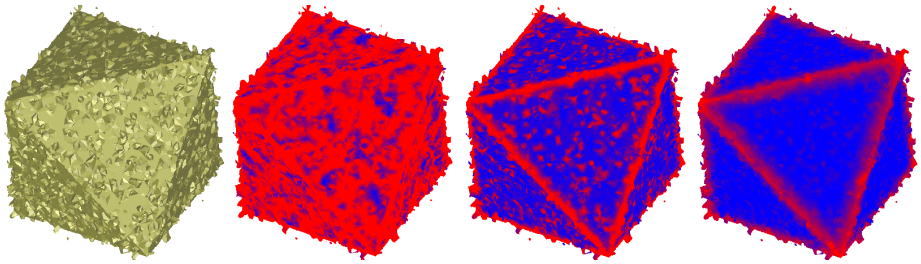

FIG. 8.1. Curvature evaluation of the noisy octahedron levelset resolved on a 64^3 grid is compared with respect to different stencil widths of the L^2 projection. From left to right the noisy level set and curvature evaluation with stencil widths $l = 2, 4$, and 8, respectively, are shown. A color ramp from blue to red indicates the dominant curvature.

Balancing of the two error terms leads to an optimal choice of $\sigma = h^{\frac{2}{3}}$ in case of a smooth function ϕ, whereas for σ sufficiently small the first term will be dominant. Thus we recognize that the width of our stencil $\mathcal{B}_\sigma(x)$ should increase significantly with decreasing grid size to ensure consistency. Nevertheless this is unrealistic in true image processing applications with non smooth intensity and steep transitions, hence we have to fix the stencil width somehow. From our experience a suitable value is $l = 4$, i.e. $\sigma = 4\,h$.

As mentioned above, we expect our third regularization approach to behave similar to the convolution method in terms of the relation between filter width and grid size. To analyze the consistency of our implementation experimentally, we have considered the spherical level sets of the image $\phi(x) := \|x - r\|, r = (R, R, R)^T$ for a fixed $R \in \mathbb{R}$ and defined an error

$$e_i := \left\| \kappa_i^\sigma - \frac{1}{R} \right\|_{L^2(\Omega_\sigma)},$$

that is the L^2 norm of the difference between κ_i and the real curvature $1/R$ of the spherical level sets. In our computation we set $\Omega := [0,1]^3$ and assume $\Omega_\sigma := \{x \in \Omega \,|\, \mathrm{dist}(x, \partial\Omega) > 1/4\}$. This turns out to be the maximum subset of Ω such that the considered projection stencil is always completely contained in Ω for every $x \in \Omega_\sigma$. In Table 8.1 we collect for three different grid widths h, fixed $R = 4$ and increasing size l of the projection stencil the values of e_i.

For l sufficiently small we expect $\frac{h^2}{\sigma^2}$ to be the dominant term in our consistency analysis above. Thus, recalling that $\sigma = l\,h$, we should observe for a doubling the stencil width l a decrease of the errors approximately by a factor $1/4$. In addition we observe that for fixed l the error is more or less independent of the grid size h.

Furthermore, we test the invariance property known for the continuous model in case of our numerical implementation. Therefore, we study ellipsoidal level sets defined by a quadratic polynomial image function ϕ_0 interpolated on the grid nodes. We observe that the relative loss of volume of the considered level sets is in the range of interpolation errors. Moreover in an application (cf. Fig. 5.3 and 5.4) we recognize that the isotropic Perona Malik method as well as the Mean Curvature Motion approach decrease the considered sub volume during the evolution about ten times faster the new anisotropic geometric diffusion method.

9. Parametric versus level set approach. Besides the general difference that the new level set method propagates all level sets on a given image simultaneously and the parametric model (cf. Section 4) deals with a single surface, the two models behave surprisingly different

TABLE 8.1
Consistency errors for different sizes of h and increasing stencil width l of the L^2 projection.

h	l	e_1	e_2
1/32	2	5.451e-02	5.451e-02
	4	1.398e-02	1.398e-02
	8	3.517e-03	3.517e-03
	16	8.806e-04	8.806e-04
1/64	2	5.479e-02	5.479e-02
	4	1.405e-02	1.405e-02
	8	3.535e-03	3.535e-03
	16	8.852e-04	8.852e-04
	32	2.214e-04	2.214e-04

h	l	e_1	e_2
1/128	2	5.493e-02	5.493e-02
	4	1.409e-02	1.409e-02
	8	3.544e-03	3.544e-03
	16	8.875e-04	8.875e-04
	32	2.220e-04	2.220e-04
	64	5.549e-05	5.549e-05

concerning the actual propagation velocity although the considered diffusion tensors are very closely related.

The parametric surface processing problem discussed in Section 4 is characterized by a speed of propagation V of a single surface $\mathcal{M}$ which splits into a tangential and a normal component, i. e.

$$V = V_{\text{tang}} - \text{tr}(a^\sigma_{\mathcal{T}_x\mathcal{M}} \circ S_{\mathcal{T}_x\mathcal{M}})N$$

where V_{tang} is the tangential component (cf. [10]). In case of mean curvature motion where $a^\sigma_{\mathcal{T}_x\mathcal{M}} = \text{Id}|_{\mathcal{T}_x\mathcal{M}}$ the propagation is in normal direction, i. e. V_{tang} vanishes. But for anisotropic geometric diffusion this tangential dislocation turns out to be a shortcoming in the corresponding numerical implementation although it effectively does not change the continuous evolution. Indeed it leads to a stretching of a triangular finite element mesh in the neighborhood of edges on the surface. In comparison to this model, the level set method presented here by its nature considers only propagation in normal direction and we avoid the problem of tangential dislocation. As propagation speed V one obtains

$$V = f\,N = (\,\text{tr}(a^\sigma(S_\sigma - S)) + (\text{div}\; a^\sigma)(N^\sigma - N)\,)\;N\,.$$

Hence, the speed in the parametric model measures the anisotropic mean curvature, whereas the speed in the level set method mainly depends on an anisotropically weighted difference of prefiltered and actual curvatures, given by the corresponding shape operators. This especially implies the above stated invariance of the level set method for ellipsoidal shapes defined as level sets of a quadratic polynomial. In contrast to that, generalized minimal surfaces with $H_{a^\sigma} = 0$ are the only invariant surfaces under the parametric evolution. Indeed, there is no compact invariant surface embedded in $\mathbb{R}^3$.

The precise counterpart of the parametric model in the level set context is given by the evolution equation

$$\partial_t\phi - \|\nabla\phi\|\,\text{tr}(a^\sigma\,S) = 0\,.$$

But, we can also adapt the parametric evolution to the new model, introduced here in the level set context. Thus, we consider a parametric evolution described by the equation

$$\partial_t x - \text{div}_{\mathcal{M}(t)}(a^\sigma_{\mathcal{T}_x\mathcal{M}}\,\nabla_{\mathcal{M}(t)}x) = r\,,$$

where we define a local averaged forcing $r = \mathrm{tr}(a^\sigma_{\mathcal{T}_x\mathcal{M}} \circ S^\sigma_{\mathcal{T}_x\mathcal{M}})$ for a convoluted shape operator $S^\sigma_{\mathcal{T}_x\mathcal{M}}$. Let us underline that this can be regarded as a local version of the global volume conservation model proposed in [10] where $r = \frac{1}{|\mathcal{M}|}\int_M \mathrm{tr}(a^\sigma_{\mathcal{T}_x\mathcal{M}} \circ S_{\mathcal{T}_x\mathcal{M}})$.

Although, originally designed for 3D image data we could also apply the presented level set method to parametric surfaces as input data as they frequently appear in computer graphics. To this end, we have to convert the parametric representation to an implicit one via the computation of a discrete approximation of the signed distance function [33], run the algorithm, and finally extract again a triangulation from the volume data set via some marching cube method or process the surface further in volumetric form.

10. Conclusions. We have presented a level set method for generalized geometric diffusion in 3D image processing. The corresponding evolution equation invokes mainly geometric quantities of level sets of the image intensity. This classifies the approach as a morphological scale space method. It is able to successively smooth noisy initial data while simultaneously retaining edges and corners on the level sets, which are characterized by considerably large principal curvatures. The evaluation of the shape operator, the surface normal, and tangent space respectively is based on a prefiltering of the noisy initial data. Thereby, the proposed method of choice is a local L^2 projection onto the space of quadratic polynomials. The corresponding nonlinear partial differential equation has been discretized by finite elements in space and a semi implicit backward Euler scheme in time. In each time step only a sparse system of linear equations has to be solved. The user controls the surface evolution mainly by two parameters — the prefilter width σ and the threshold λ — which both have an intuitive meaning. The method comes along with a geometric interpretation of the propagation speed of level sets and a large set of invariant shapes. In fact the invariance principle for level sets of second order polynomials and the edge indicating shape operator as a second order differential operator on the level sets give reason for the essential characteristics of the described method. Interesting future research directions are

- to study the actual counterpart of the parametric surface processing model in level set form and vice versa,
- to generalize the method for inpainting or restoration purposes on 3D images,
- and to expand the evolution problem by considering additional terms in the propagation speed, which allow a more general modeling of the level sets.

Acknowledgments. We thank Ulrich Clarenz, Gerd Dziuk and Joachim Weickert for inspiring discussions and helpful comments on the topic. The echocardiographical data show in Figures 1.1 and 5.2 was provided by TomTec Imaging Systems and C. Lamberti from DEIS, Bologna University. Furthermore we acknowledge Sascha Oswald from Sheffield University, who performed the fresh and salt water experiments shown in Figures 5.3, 5.4, 5.5 and 5.6. For the computations according the parametric surface processing model we thank Udo Diewald from Bonn University (cf. [10]).

REFERENCES

[1] L. Alvarez, F. Guichard, P. L. Lions, and J. M. Morel. Axioms and fundamental equations of image processing. *Arch. Ration. Mech. Anal.*, 123(3):199–257, 1993.

[2] S. B. Angenent and M. E. Gurtin. Multiphase thermomechanics with interfacial structure 2, evolution of an is othermal interface. *Arch. Rational Mech. Anal.*, 108:323–391, 1989.

[3] E. Bänsch and K. Mikula. A coarsening finite element strategy in image selective smoothing. *Computing and Visualization in Science*, 1:53–63, 1997.

[4] G. Bellettini and M. Paolini. Anisotropic motion by mean curvature in the context of finsler geometry. *Hokkaido Math. J.*, 25:537–566, 1996.

[5] R. A. Carmona and S. Zhong. Adaptive smoothing respecting feature directions. *IEEE Transactions on Image Processing*, 7(3):353–358, 1998.
[6] F. Catté, P.-L. Lions, J.-M. Morel, and T. Coll. Image selective smoothing and edge detection by nonlinear diffusion. *SIAM J. Numer. Anal.*, 29(1):182–193, 1992.
[7] I. Chavel. *Eigenvalues in Riemannian Geometry*. Academic Press, 1984.
[8] Y.-G. Chen, Y. Giga, and S. Goto. Uniqueness and existence of viscosity solutions of generalized mean curvature flow equations. *J. Diff. Geom.*, 33(3):749–786, 1991.
[9] P. Ciarlet and J. Lions. *Handbook of numerical analysis. Vol. V: Techniques of scientific computing*. Elsevier, 1997.
[10] U. Clarenz, U. Diewald, and M. Rumpf. Nonlinear anisotropic diffusion in surface processing. In *Proc. Visualization 2000*, pages 397–405, 2000.
[11] K. Deckelnick and G. Dziuk. Discrete anisotropic curvature flow of graphs. *Mathematical Modelling and Numerical Analysis, to appear*, 2000.
[12] K. Deckelnick and G. Dziuk. A fully discrete numerical scheme for weighted mean curvature flow. Technical Report 30, Mathematische Fakultät Freiburg, 2000.
[13] M. Desbrun, M. Meyer, P. Schroeder, and A. Barr. Implicit fairing of irregular meshes using diffusion and curvature flow. In *Computer Graphics (SIGGRAPH '99 Proceedings)*, pages 317–324, 1999.
[14] M. P. do Carmo. *Riemannian Geometry*. Birkhäuser, Boston–Basel–Berlin, 1993.
[15] G. Dziuk. An algorithm for evolutionary surfaces. *Numer. Math.*, 58:603–611, 1991.
[16] L. Evans and J. Spruck. Motion of level sets by mean curvature I. *J. Diff. Geom.*, 33(3):635–681, 1991.
[17] G. Huisken. The volume preserving mean curvature flow. *J. Reine Angew. Math.*, 382:35–48, 1987.
[18] J. Kačur and K. Mikula. Solution of nonlinear diffusion appearing in image smoothing and edge detection. *Appl. Numer. Math.*, 17 (1):47–59, 1995.
[19] B. Kawohl and N. Kutev. Maximum and comparison principle for one-dimensional anisotropic diffusion. *Math. Ann.*, 311 (1):107–123, 1998.
[20] R. Kimmel. Intrinsic scale space for images on surfaces: The geodesic curvature flow. *Graphical Models and Image Processing*, 59(5):365–372, 1997.
[21] L. Kobbelt. Discrete fairing. In *Proceedings of the 7th IMA Conference on the Mathematics of Surfaces*, pages 101–131, 1997.
[22] L. Kobbelt, S. Campagna, J. Vorsatz, and H.-P. Seidel. Interactive multi-resolution modeling on arbitrary meshes. In *Computer Graphics (SIGGRAPH '98 Proceedings)*, pages 105–114, 1998.
[23] R. Malladi and J. A. Sethian. Image processing: Flows under min/max curvature and mean curvature. *Graphical Models and Image Processing*, 58(2):127–141, March 1996.
[24] K. Mikula and J. Kačur. Evolution of convex plane curves describing anisotropic motions of phase interfaces. *SIAM Journal on Scientific Computing*, 17(6):1302–1327, 1996.
[25] J.-M. Morel and S. Solimini. *Variational Methods in Image Segmentation*. Birkhauser, 1995.
[26] E. Pauwels, P. Fiddelaers, and L. Van Gool. Enhancement of planar shape through optimization of functionals for curves. *IEEE Trans. Pattern Anal. Mach. Intell.*, 17:1101–1105, 1995.
[27] P. Perona and J. Malik. Scale space and edge detection using anisotropic diffusion. In *IEEE Computer Society Workshop on Computer Vision*, 1987.
[28] T. Preußer and M. Rumpf. Anisotropic nonlinear diffusion in flow visualization. In *Proceedings Visualization 1999*, pages 325–332, 1999.
[29] T. Preußer and M. Rumpf. An adaptive finite element method for large scale image processing. *Journal of Visual Comm. and Image Repres.*, 11:183–195, 2000.
[30] G. Sapiro. Vector (self) snakes: A geometric framework for color, texture, and multiscale image segmentation. In *Proc. IEEE International Conference on Image Processing, Lausanne*, September 1996.
[31] A. Schmidt. Computation of three dimensional dendrites with finite elements. *Journal of Computational Physics*, 125:293–312, 1996.
[32] C. Schnoerr. A study of a convex variational diffusion approach for image segmentation and feature extraction. *J. Math. Imaging Vis.*, 8(3):271–292, 1998.
[33] J. A. Sethian. *Level Set Methods and Fast Marching Methods: Evolving Interfaces in Geometry, Fluid Mechanics, Computer Vision and Materials Sciences*. Cambridge Univ. Press, 1996.
[34] J. A. Sethian. *Level Set Methods and Fast Marching Methods*. Cambridge University Press, 1999.
[35] G. Taubin. A signal processing approach to fair surface design. In *Computer Graphics (SIGGRAPH '95 Proceedings)*, pages 351–358, 1995.
[36] J. E. Taylor, J. W. Cahn, and C. A. Handwerker. Geometric models of crystal growth. *Acta metall. mater.*, 40:1443–1474, 1992.
[37] V. Thomee. *Galerkin - Finite Element Methods for Parabolic Problems*. Springer, 1984.
[38] J. Weickert. Theoretical foundations of anisotropic diffusion in image processing. *Computing*, Suppl. 11:221–236, 1996.
[39] J. Weickert. *Anisotropic diffusion in image processing*. Teubner, 1998.